ISSN 0021-3640, JETP Letters, 2018, Vol. 107, No. 1, pp. 42–47. © Pleiades Publishing, Inc., 2018.
Original Russian Text © T.E. Kuzmicheva, S.A. Kuzmichev, A.A. Kordyuk, V.M. Pudalov, 2018, published in Pis'ma v Zhurnal Eksperimental'noi i Teoreticheskoi Fiziki, 2018, Vol. 107, No. 1, pp. 47–53.

CONDENSED MATTER

Structure and Anisotropy of the Superconducting Order Parameter in $Ba_{0.65}K_{0.35}Fe_2As_2$ Probed by Andreev Spectroscopy[1]

T. E. Kuzmicheva[a, *], S. A. Kuzmichev[a, b], A. A. Kordyuk[c], and V. M. Pudalov[a, d]

[a] *Lebedev Physical Institute, Russian Academy of Sciences, Moscow, 119991 Russia*
[b] *Moscow State University, Moscow, 119991 Russia*
[c] *Kurdyumov Institute for Metal Physics, National Academy of Sciences of Ukraine, Kyiv, 03142 Ukraine*
[d] *National Research University Higher School of Economics, Moscow, 101000 Russia*
**e-mail: kute@sci.lebedev.ru*

Received November 2, 2017; in final form, November 16, 2017

The superconducting order parameters in optimally doped $Ba_{0.65}K_{0.35}Fe_2As_2$ single crystals have been directly measured using multiple Andreev reflection effect spectroscopy of superconductor–normal metal–superconductor break-junctions. We determine two superconducting gaps, which are nodeless in the k_xk_y-plane of the momentum space, and resolve a substantial in-plane anisotropy of the large gap. The temperature dependences of the gaps indicate a strong coupling within the bands where Δ_L develops, a weak coupling in the condensate with the small gap Δ_S, and a moderate interband interaction between the two condensates. The own critical temperatures of both condensates have been estimated (under the hypothetical assumption of zero interband interaction).

DOI: 10.1134/S002136401801006X

Superconducting compounds belonging to the $BaFe_2As_2$ pnictide family show a moderate critical temperature up to 38 K upon hole doping, in particular, by substitution of K for Ba. Large high quality single crystals with variable composition are easily grown, facilitating intensive studies of the properties of these compounds. The structure of the Ba-122 pnictides contains superconducting FeAs blocks separated with Ba blocks along the c axis. As compared to the 1111, 24622, or 32522 pnictide families which quasi-two-dimensionality resembles that in cuprates, the Ba-122 compounds, have more isotropic (in-plane to out-of-plane) transport and magnetic properties. In the optimally doped $Ba_{0.65}K_{0.35}Fe_2As_2$ samples, angle-resolved photoemission spectroscopy (ARPES) studies [1, 2] showed the presence of four bands crossing the Fermi level, one electron-like, and three hole-like bands. The Fermi surface comprises two concentric hole-like barrels near the Γ point, and the electron-like cylinder surrounded by four hole-like "blades" forming a propeller-like structure near the X point of the Brillouin zone. At temperatures below T_c, two superconducting condensates coexist. As follows from the ARPES data [1, 2], the small gap with $2\Delta_S/k_BT_c \sim 1$ opens at the outer Γ barrel, whereas the single large gap with $2\Delta_L/k_BT_c \sim 6.8$ opens at all other parts of the Fermi surface. A variety of pairing symmetries with nodeless, nodal or anisotropic gaps were discussed from theoretical point of view [3–5].

Although the two-gap superconductivity in the Ba-122 family seems unambiguously established, the superconducting gap values determined by various techniques are highly contradictory. Possibly, this may be caused by lacking of direct probes, or limited (insufficient) resolution of experimental techniques, as well as by intrinsic features of these materials, such as significant influence of surface states [6], both in-plane and out-of-plane gap anisotropy (considered, e.g., in [3, 4]), proximity to Lifshitz transition [5], or interplay between the superconducting and magnetic properties. As a result, for Ba-122 pnictides, the reported in literature characteristic ratio for the large "driving" gap varies from 4 to even 11 (for a review, see [1, 2, 7, 8]). From this brief overview, it becomes evident that direct and self-consistent experimental data are crucial in order to uncover the pairing mechanism in Ba-122 pnictides.

Here, we present a direct study of the superconducting order parameter in optimally doped $Ba_{0.65}K_{0.35}Fe_2As_2$ using multiple Andreev reflection effect spectroscopy of superconductor–normal metal–superconductor (SNS) break-junctions. We determine magnitudes of the two superconducting gaps, show the absence of nodes in the k_xk_y-plane of

[1] The article was translated by the authors.

the momentum space, and resolve a substantial in-plane anisotropy of the large gap. Based on the measured temperature dependences of the gaps, we estimate the own critical temperatures of the two condensates, and interband interaction.

The large size $Ba_{0.65}K_{0.35}Fe_2As_2$ single crystals were synthesized by self-flux technique using FeAs as the flux, for details see [9]. The chemical composition, crystal structure and lattice parameters were tested by X-ray diffractometer (Pan Analytical X'Pert Pro MRD), and scanning electron microscope JEOL JSM-7001 equipped with an energy dispersive X-ray (EDX) spectroscopy probe. The critical temperature of the superconducting transition $T_c = (36.5 \pm 0.2)$ K was determined from magnetization and DC transport measurements [9, 10].

In order to directly determine the structure of the superconducting order parameter and its temperature dependence, we used Andreev spectroscopy of SNS junctions. The multiple Andreev reflection effect (MARE) is observed in the SNS ballistic contact (whose diameter $2a$ is less than the carrier mean free path l [11]). The multiple Andreev reflection effect causes an excess current in current–voltage characteristic (CVC), which significantly grows in low-bias region (the so-called foot area). A series of dynamic conductance features (subharmonic gap structure (SGS)) appears at bias voltages $V_n = \frac{2\Delta}{en}$, (where n is a natural number) [12–15]. This simple expression enables to determine directly the superconducting gap value at any temperatures up to T_c [12, 15]. For the high-transparency SNS Andreev regime (typical for our break-junction contacts), SGS reveals itself as a series of dips for both nodeless and nodal superconducting energy gap. The coexistence of two superconducting gaps would cause, obviously, two SGS's in the $dI(V)/dV$ spectrum. A k-space angular dependence of the gap value strongly affects the SGS lineshape. In case of isotropic gap, the SGS minima are sharp and symmetrical, whereas a nodal gap leads to less intensive and asymmetric $dI(V)/dV$ minima [16, 17]. For the extended s-wave nodeless gap, the SGS demonstrates doublet minima corresponding to the two extremal values of the anisotropic gap [8, 18].

For Andreev spectroscopy studies, we used a break-junction (BJ) technique (for details, see [18–21]) in order to fabricate the symmetric SNS contacts. In the break-junction experiment, the studied sample is precisely cleaved in the cryogenic environment (Fig. 1). The single crystal prepared as a thin $3 \times 1.5 \times 0.1$-mm plate was attached to a springy holder by four In–Ga pads (liquid at room temperature) which insured true 4-probe connection and helped aligning the ab-plane parallel to the sample holder. After cooling down to 4.2 K, the sample holder was precisely bent; this caused cracking of the single crystal. The resultant microcrack represents the superconductor–

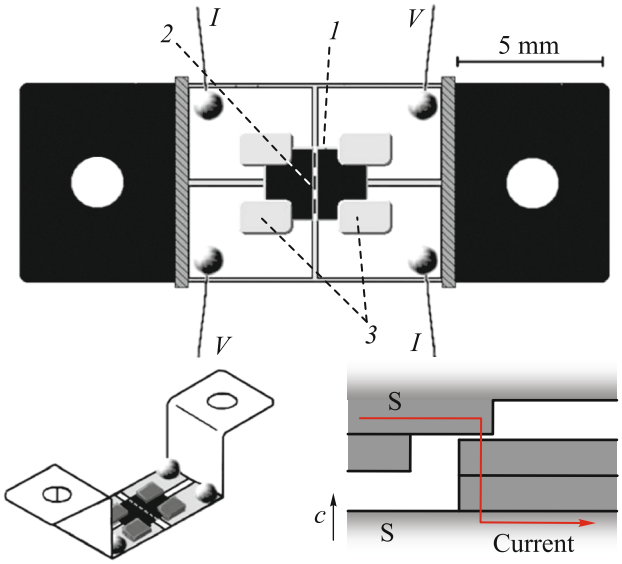

Fig. 1. (Color online) Sample mounting on the holder in the break-junction experiment, and the schematic of the break junction formation in a layered single crystal: (*1*) sample, (*2*) microcrack, and (*3*) In–Ga pads. The arrow shows the bias current direction (along the c axis) through the array.

constriction–superconductor contact, where the constriction acts as a weak link.

In our setup, the superconducting banks of the crack slide in the ab-plane and are closely touching each other [18]. As a result, the metallic Ba-blocks between the superconducting Fe–As blocks of the crystal structure, form highly transparent weak links. Therefore, the observed $I(V)$ and $dI(V)/dV$ characteristics of the break junctions in Ba-122 are typical for high transparency Andreev transport mode [12–15]. Since in our setup the microcrack is located deep in the bulk of the sample and away from the current leads, the cryogenic clefts are protected from Joule overheating or degradation.

In layered samples, the break-junction technique often forms also natural arrays of the SNSN-...-S-type realized at the steps and terraces. As an example, Fig. 1 schematically illustrates formation of the array between the surface of the cryogenic cleft and the step. The current always flows through the array along the c crystallographic axis. In such array, an intrinsic multiple Andreev reflections effect (IMARE) occurs. This effect is similar to the intrinsic Josephson effect and is observed in all layered superconductors (for a review, see [18, 20]). The Andreev array consists of sequence of m SNS junctions; therefore, SGS appears at positions enlarged by a factor of m, i.e., $V_n = 2\Delta \times m/en$. In general, the positions of any other peculiarities caused by *bulk* properties of material also scale with m. In our experiment, we were able to probe tens of single SNS contacts and arrays (containing various number of

junctions m) by precisely readjusting the microcrack. The latter opportunity enables one to collect a large amount of data and to check reproducibility of the *bulk* gap values and other *bulk* properties of the material. The number of junctions m in the array can be determined as a natural number that scales the bias voltage to make the position of the bulk-caused features coinciding with those for the single SNS contact.

The high quality of the break-junctions enables to study the true bulk properties of the sample and to minimize the influence of the surface states (which seem to be significant for Ba-122 [6]) *locally*, i.e., within the contact size $2a \approx 5$–30 nm. These features favor direct and high-precision measurement of the superconducting gap and its temperature dependence. The break-junction technique enables also resolving fine structure of $dI(V)/dV$, in particular, for probing the gap anisotropy. We note that in our set-up, the carriers with various momenta in the k_xk_y-plane pass ballistically through the constriction along the c-direction, with the velocity $v_c \ll v_a, v_b$ Therefore, this technique ensures observation only of the k_xk_y-plane anisotropy [8, 18].

Figure 2a shows typical $dI(V)/dV$ characteristics (measured at $T = 4.2$ K) for natural SNSNS arrays ($m = 2$ SNS junctions). The corresponding $I(V)$ curves are shown in the inset. Regardless of the notably different contact resistance, the position of the main features of the dynamic conductance remains constant (see Figs. 2a, 2b). The pronounced foot at low bias voltages signals that the constriction formally behaves like a normal metal with a high transparency (95–98%) and ballistic c-axis transport [12–15].

In order to estimate the actual diameter of the constriction, we take the product of the normal in-plane resistivity and effective elastic mean free path $\rho^{ab}l^{el} \approx 3.5\times10^{-11}$ Ω cm^2 [9], and the contact resistance $R = 38$ Ω. Using the Sharvin's formula [11], one gets $2a = 2\sqrt{4\rho^{ab}l^{el}/3\pi R} \approx 12$ nm. Taking account of the partial Fermi momenta and conductivities for the four bands crossing the Fermi level, determined for nearly optimal (Ba, K)Fe_2As_2 crystal from the same batch in ARPES and transport measurements [1, 2, 9], we get the elastic mean free path up to 10–30 nm. This rough estimate gives $2a \le l^{el}$ consistent with the MARE condition for observing $n = 1$–2 Andreev subharmonics in the dynamic conductance spectrum [15]. Generally speaking, for observation of MARE the contact diameter should be less than the inelastic mean free path, which usually exceeds l^{el} by several times. Taking the latter into account, we conclude the conditions are fulfilled for observation of MARE in the high transparency regime.

The $dI(V)/dV$ spectra in Fig. 2a show a set of dynamic conductance dips typical for clean SNS contacts. In order to normalize the $I(V)$ and $dI(V)/dV$ spectra to those for a single junction, the voltage axis was scaled by a factor of $m = 2$. The large gap SGS starts with the pronounced dips at $eV \approx 18.5$ meV corresponding to $2\Delta_L$ in accordance with the SGS expression. The spectrum has no more features at higher bias, up to ±35 mV, therefore the dips at ±18.5 meV are the main harmonic ($n = 1$) for the large gap. The features at $V \approx \pm11.5$ mV do not match the expected position ($\approx \pm9$ mV) of the second subharmonic of the large gap, therefore these two dips at ±18.5 and ±11.5 mV may be interpreted as a doublet $n = 1$ feature of the large gap. The gap anisotropy may be determined as $(1 - \Delta_L^{in}/\Delta_L^{out}) \approx 33\%$, where Δ_L^{in} and Δ_L^{out} are the extrema of the large gap angular distribution corresponding to the inner and outer dips of the doublet, respectively. The positions of the next pair of dynamic conductance features, $V \approx \pm9.6$ and ±6.4 mV, correspond to the second subharmonic of Δ_L. Note that the $n = 2$ doublet is exactly half as narrow as the $n = 1$ doublet, in agreement with the expression for SGS. As shown in the inset, such doublets are reproducibly observed in the $dI(V)/dV$ spectra of $Ba_{0.65}K_{0.35}Fe_2As_2$ at $T = 4.2$ K (the lower curves), and remain also resolved upon increasing temperature up to, at least, $T \approx 16$ K $\sim T_c/2$ (the upper curve). The positions of both minima in the doublet are stable and independent of the constriction size or resistance, thus the observed splitting of features cannot be attributed to the size effects.

To say unambiguously whether the $dI(V)/dV$ doublets are caused by the anisotropy in the k_xk_y-plane, or by the coexistence of two gaps with close values, one needs detailed analysis of the Andreev feature lineshape. Nevertheless, the intensity and the lineshape of the doublets is undoubtedly inconsistent with that expected for the d-wave or fully anisotropic (nodal) s-wave symmetry [16, 18]; we conclude therefore that the large gap is nodeless in the k_xk_y plane. On the other hand, it should be taken into consideration that the ARPES studies have not revealed the presence of the third gap $\Delta \sim 6.4$ meV, whereas similar anisotropy was resolved in our earlier IMARE studies of the Ba-122 with various composition [8, 17, 22, 23]. Taking the above into account, we conclude the extended s-wave is the most likely symmetry of the large gap. The extremal amplitude of the large gap angular distribution are $\Delta_L^{in} \approx 6.4$ meV (inner), and $\Delta_L^{out} \approx 9.5$ meV (outer). The middle range of the characteristic ratio $2\Delta_L/k_BT_c \approx 4.1$–$6.1$ is the same as that for the 1111 compounds determined in our previous studies [18, 20].

At lower biases, a second SGS (related with the small gap) is observed in the dynamic conductance spectra. Figure 2b shows low-bias fragments of

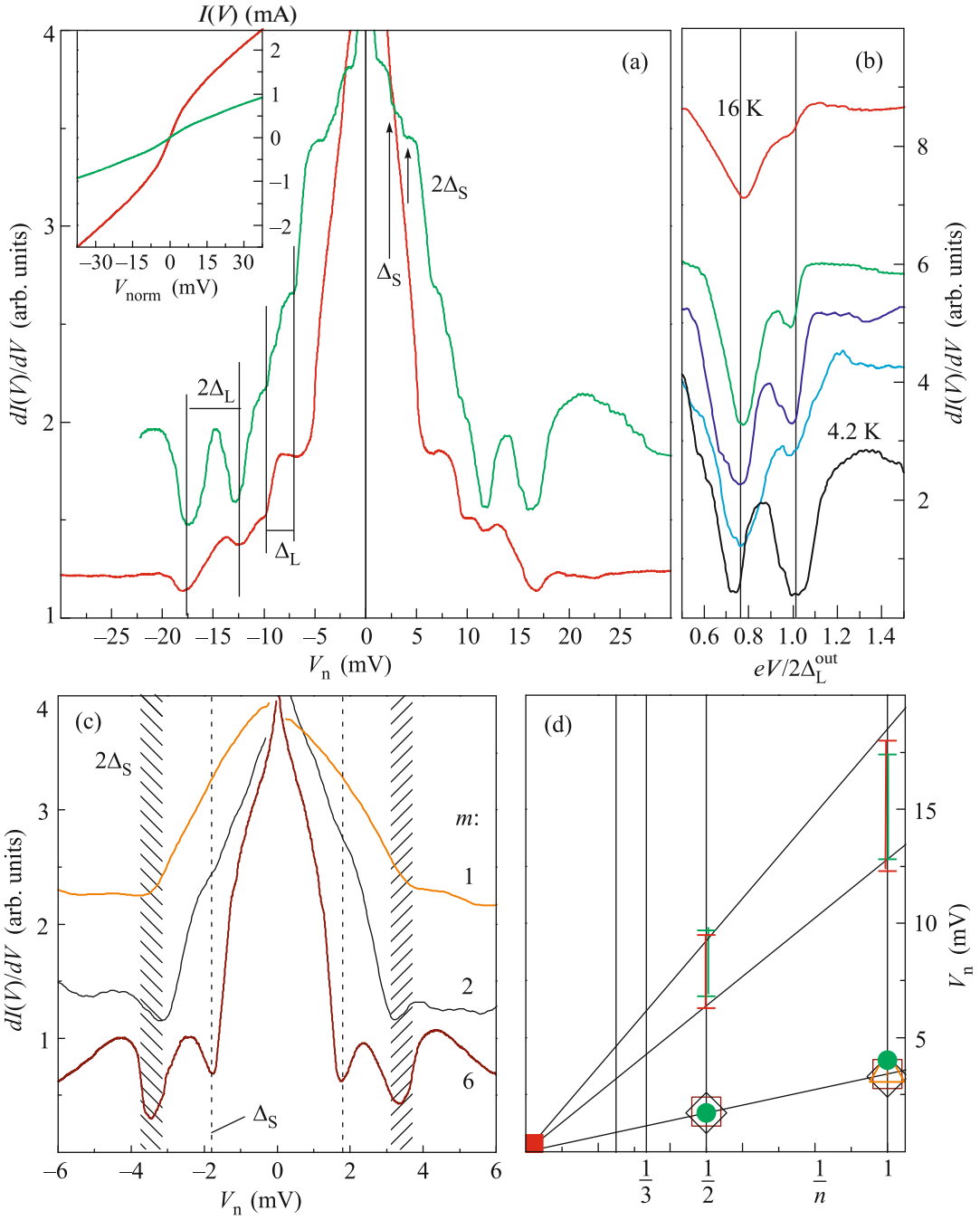

Fig. 2. (Color online) (a) Dynamic conductance spectra for Andreev arrays measured at $T = 4.2$ K. Black vertical lines depict positions of the Andreev subharmonics determining the edge values $\Delta_L \approx 6.4$ and 9.5 meV (≈33% anisotropy in the k_xk_y-plane). The arrows show the small gap subharmonics. The inset shows CVCs of these contacts. (b) Doublet structure of the large gap observed in $dI(V)/dV$ for various Andreev arrays at 4.2 and (upper curve) 16 K. (c) Low-bias fragments of dynamic conductance spectra of ($m = 2,6$ junctions, the lower curves) Andreev arrays and (upper curve) a single SNS junction demonstrating SGS of the small gap $\Delta_S \approx 1.8$ meV (hatched areas and dashed vertical lines). (d) Positions of (vertical bars depict the gap anisotropy) Δ_L and (open symbols) Δ_S features in the $dI(V)/dV$ spectra shown in panels (a, c), versus their inverse number $1/n$.

dynamic conductance spectra for $m = 6,2$ Andreev arrays, and for a single SNS junction. The width and the slope of the foot near zero bias are reproducible for all the curves. The minima at $eV \approx 3.5$ meV and at $eV \approx 1.8$ meV correspond to the first ($n = 1$) and second ($n = 2$) SGS harmonics. These features obviously do not belong to the large gap; rather, they originate from a small gap $\Delta_S \approx 1.8$ meV. Unlike the Δ_L dou-

blets, the small gap peculiarities are not split but rather symmetric, thus pointing to nearly isotropic Δ_S in the k-space. The positions of Δ_S features are reproducible, although the data shown in Fig. 2b are obtained for Andreev contacts with different resistance. The minima become sharper as number of contacts in the array m increases. Such a characteristic property of the results obtained by IMARE spectroscopy [18, 20, 21] proves diminishing contribution of the surface defects to conduction, and, hence, the bulk origin of the Δ_S order parameter.

Using the data presented in Figs. 2a and 2b, the SGS positions V_n are plotted in Fig. 2c versus their inverse number $1/n$. According to the SGS expression $eV_{n,i} = 2\Delta_i/n$ (where i = L, S), V_n should depend linearly on $1/n$ and tend to zero at $n \to \infty$. The resulting straight lines passing through three points (the positions V_n of the first and the second harmonics, as well as the origin) unambiguously demonstrate the existence of two distinct superconducting condensates characterized with the order parameters Δ_L and Δ_S. The determined large and small gaps agree well with measurements of the lower critical field [22], and ARPES data [1, 2] obtained with the crystals from the same batch.

The directly measured temperature dependences of the gaps are shown in Fig. 3. For the large gap, both the inner and outer extrema are resolved at low temperatures. The splitting of the Δ_L doublets remains almost constant, as shown in the inset. With temperature increasing, the inner dip of the doublet smears, whereas the outer $\Delta_L^{out}(T)$ is resolved until the local critical temperature of the junction. The estimated gap anisotropy $1 - \Delta_L^{in}/\Delta_L^{out} \approx 36\%$ is unchanged practically with temperature.

A single-band model is obviously inconsistent with the experimentally measured temperature dependences of the large and the small gaps. The $\Delta_L(T)$ dependence passes somewhat below the single-band BCS-like curve (dash-dotted line), whereas $\Delta_S(T)$ bends down significantly. The different temperature dependences of the two gaps confirms the coexistence of two independent order parameters, Δ_L and Δ_S. On the other hand, the doublet $\Delta_L^{out}(T)$ and $\Delta_L^{in}(T)$ temperature dependences are similar, at least until $T \approx T_c^{local}/3$, and describe therefore properties of the same condensate.

Taking into account the three strongly coupled bands where the anisotropic large gap develops, one can consider them as an effective "driving" condensate with the Δ_L order parameter. The experimental $\Delta_{L,S}(T)$ dependences are obviously typical for a moderate interband interaction between the effective Δ_L and Δ_S bands. Therefore, as a rough estimate, a two-band model is suitable to determine the own characteristic ratio for each condensate, i.e., $2\Delta_i/k_BT_c^i$ (i = L,S) expected in the hypothetical case of zero interband coupling. The experimental $\Delta_{L,S}(T)$ dependences could be fit with a two-band model based on Moskalenko and Suhl system of equations with the renormalized BCS integral [24–28] (solid lines in Fig. 3). As a result, both gaps are expected to become zero at the same temperature $T_c^{local} \approx 36$ K which corresponds to the contact area (of the size $2a \approx 12$ nm) transition to the normal state. The local critical temperature is a bit lower than the bulk T_c determined at a maximum of $d\rho^{bulk}/dT$ for the bulk crystal (rhombs and dashed line in Fig. 3). Using the two-band fit, we determined a strong effective coupling in the "driving" bands with the own characteristic ratio $2\Delta_L^{out}/k_BT_c^L \approx 5.3 > 3.5$, which corresponds to the own critical temperature $T_c^L \approx 43$ K. Such T_c value could be realized for the system of driving bands in the absence of the Δ_S condensate, or in the hypothetical case of zero interaction with it. However, according to our data, the two condensates moderately interact in the k-space, which lowers the actual T_c of the compound by 20% as compared to T_c^L. At the same time, the intraband coupling for the condensate with the Δ_S order parameter, which develops at the

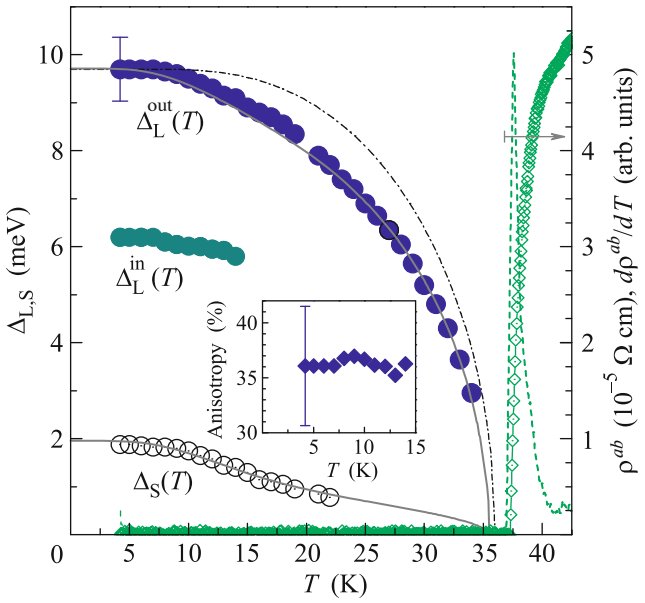

Fig. 3. (Color online) Temperature influence (solid circles) on the large gap extrema Δ_L^{out} and Δ_L^{in} and (open circles) on the small gap Δ_S. The single-band fit (dash-dotted line), two-band fit (solid lines), bulk resistance transition (rhombs), and $d\rho(T)/dT$ (dashed line) are shown for comparison. The inset shows the temperature dependence of the Δ_L anisotropy determined as $1 - \Delta_L^{in}/\Delta_L^{out}$.

outer Γ barrel [1, 2], is weak and close to the BCS-limit. Its own ratio $2\Delta_S/k_BT_c^S \approx 3.6$ leads to $T_c^S \approx 12$ K, which matches the temperature at which both $\Delta_{L,S}(T)$ dependences noticeably bend down.

In conclusion, by multiple Andreev reflection spectroscopy of $Ba_{0.65}K_{0.35}Fe_2As_2$ single crystals with $T_c \approx 36$ K, we directly determined two superconducting gaps: the anisotropic large gap Δ_L with two extremal values, 6.4 and 9.5 meV (33–36% anisotropy), and the small gap $\Delta_S = (1.8 \pm 0.3)$ meV with no signs of anisotropy, and their temperature dependences. According to our estimate, in the driving bands where the large gap develops, a strong effective coupling responsible for the high critical temperature of the compound is realized. For the hypothetical case of two noninteracting Δ_L and Δ_S condensates, the own critical temperature of the driving bands would rise up to $T_c^L \approx 43$ K. On the other hand, the intrinsic superconductivity of the small gap Δ_S band is weak and close to the BCS limit. The interband interaction between the two condensates is moderate, and causes the actual T_c of the compound to be ~20% lower than the own critical temperature T_c^L of the driving bands.

We thank H.H. Wen and H.Q. Luo for providing us with the samples. The work of T.E.K. was supported by the Council of the President of the Russian Federation for Support of Young Scientists and Leading Scientific Schools (project no. MK-5699.2016.2). The work of S.A.K. was supported by the Russian Foundation for Basic Research (project no. 15-03-99628). The work of V.M.P. was supported by the Russian Science Foundation (project no. 16-42-01100). The measurements were performed in part using research equipment of the Shared Facilities Center, Lebedev Physical Institute.

REFERENCES

1. D. V. Evtushinsky, A. A. Kordyuk, V. B. Zabolotnyy, D. S. Inosov, T. K. Kim, B. Büchner, H. Luo, Z. Wang, H.-H. Wen, G. Sun, C. Lin, and S. V. Borisenko, J. Phys. Soc. Jpn. **80**, 023710 (2011).
2. D. V. Evtushinsky, A. A. Kordyuk, V. B. Zabolotnyy, D. S. Inosov, T. K. Kim, B. Büchner, H. Luo, Z. Wang, H.-H. Wen, G. Sun, C. Lin, and S. V. Borisenko, New J. Phys. **11**, 055069 (2009).
3. P. J. Hirschfeld, C.R. Phys. **17**, 197 (2016).
4. T. Saito, S. Onari, and H. Kontani, Phys. Rev. B **88**, 045115 (2013).
5. A. Bianconi, Nat. Phys. **9**, 536 (2013).
6. E. van Heumen, J. Vuorinen, K. Koepernik, F. Massee, Y. Huang, M. Shi, J. Klei, J. Goedkoop, M. Lindroos, J. van den Brink, and M. S. Golden, Phys. Rev. Lett. **106**, 027002 (2011).
7. P. Richard, T. Qian, and H. Ding, J. Phys.: Condens. Matter **27**, 293203 (2015).
8. T. E. Kuzmicheva, V. M. Pudalov, S. A. Kuzmichev, A. V. Sadakov, Yu. A. Aleshenko, V. A. Vlasenko, V. P. Martovitsky, K. S. Pervakov, Yu. F. Eltsev, and V. M. Pudalov, Phys. Usp. **60**, 419 (2017).
9. H. Q. Luo, Z. S. Wang, H. Yang, P. Cheng, X. Y. Zhu, and H. H. Wen, Supercond. Sci. Technol. **21**, 125014 (2008).
10. S. Johnston, M. Abdel-Hafiez, L. Harnagea, V. Grinenko, D. Bombor, Y. Krupskaya, C. Hess, S. Wurmehl, A. U. B. Wolter, B. Büchner, H. Rosner, and S.-L. Drechsler, Phys. Rev. B **89**, 134507 (2014).
11. Yu. V. Sharvin and V. F. Gantmakher, Sov. Phys. JETP **38**, 604 (1974).
12. M. Octavio, M. Tinkham, G. E. Blonder, and T. M. Klapwijk, Phys. Rev. B **27**, 6739 (1983).
13. G. B. Arnold, J. Low Temp. Phys. **68**, 1 (1987).
14. D. Averin and A. Bardas, Phys. Rev. Lett. **75**, 1831(1995).
15. R. Kümmel, U. Gunsenheimer, and R. Nicolsky, Phys. Rev. B **42**, 3992 (1990).
16. T. P. Devereaux and P. Fulde, Phys. Rev. B **47**, 14638 (1993).
17. M. Abdel-Hafiez, P. J. Pereira, S. A. Kuzmichev, T. E. Kuzmicheva, V. M. Pudalov, L. Harnagea, A. A. Kordyuk, A. V. Silhanek, V. V. Moshchalkov, B. Shen, H. H. Wen, A. N. Vasiliev, and X. J. Chen, Phys. Rev. B **90**, 054524 (2014).
18. S. A. Kuzmichev and T. E. Kuzmicheva, Low Temp. Phys. **42**, 1008 (2016).
19. J. Moreland and J. W. Ekin, J. Appl. Phys. **58**, 3888 (1985).
20. T. E. Kuzmicheva, S. A. Kuzmichev, K. S. Pervakov, V. M. Pudalov, and N. D. Zhigadlo, Phys. Rev. B **95**, 094507 (2017).
21. T. E. Kuzmicheva, S. A. Kuzmichev, M. G. Mikheev, Ya. G. Ponomarev, S. N. Tchesnokov, Yu. F. Eltsev, V. M. Pudalov, K. S. Pervakov, A. V. Sadakov, A. S. Usoltsev, E. P. Khlybov, and L. F. Kulikova, Eur. Phys. Lett. **102**, 67006 (2013).
22. C. Ren, Z. S. Wang, H. Q. Luo, H. Yang, L. Shan, and H. H. Wen, Physica C **469**, 599 (2009).
23. T. E. Kuzmicheva, V. A. Vlasenko, S. Yu. Gavrilkin, S. A. Kuzmichev, K. S. Pervakov, I. V. Roshchina, and V. M. Pudalov, J. Supercond. Novel Magn. **29**, 3059 (2016).
24. V. A. Moskalenko, Fiz. Met. Metall. **8**, 522 (1959).
25. V. A. Moskalenko, Sov. Phys. Usp. **17**, 450 (1974).
26. H. Suhl, B. T. Matthias, and L. R. Walker, Phys. Rev. Lett. **3**, 552 (1959).
27. S. A. Kuzmichev, T. E. Kuzmicheva, and S. N. Tchesnokov, JETP Lett. **99**, 295 (2014).
28. S. A. Kuzmichev, T. E. Kuzmicheva, S. N. Tchesnokov, V. M. Pudalov, and A. N. Vasiliev, J. Supercond. Novel Magn. **29**, 1111 (2016).